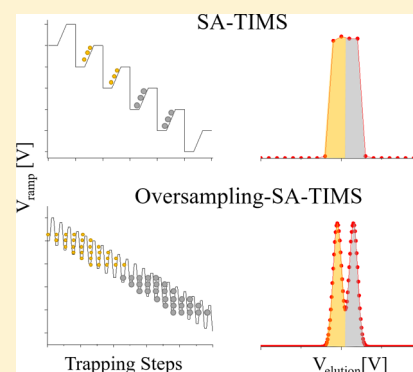


Oversampling Selective Accumulation Trapped Ion Mobility Spectrometry Coupled to FT-ICR MS: Fundamentals and Applications

Paolo Benigni[†] and Francisco Fernandez-Lima^{*,†,‡}[†]Department of Chemistry and Biochemistry and [‡]Biomolecular Sciences Institute, Florida International University, Miami, Florida 33199, United States

Supporting Information

ABSTRACT: In the present paper, we describe the fundamentals and analytical advantages of Oversampling Selective Accumulation Trapped Ion Mobility Spectrometry (OSA-TIMS) when coupled to ultrahigh resolution mass analyzers (e.g., FT-ICR MS). During TIMS analysis, ion packages are spatially resolved based on their mobilities along the TIMS analyzer axis and multiple strategies can be utilized during the trapping and elution of the ion population of interest. In the case of OSA-TIMS-FT-ICR MS, the TIMS operation sequence, trapping conditions, and operations are optimized to increase the signal-to-noise and the number of points across the mobility domain, which leads to more accurate mobility and mass measurements. Experimental results show that accurate ion-neutral collision cross sections (<1%) can be measured using OSA-TIMS-FT-ICR MS with high mobility resolving powers (R_{IMS} up to 250), high mass accuracy (<1 ppm), and ultrahigh mass resolution (R_{MS} up to 600–1200k at m/z 400) in a single analysis. The analytical advantages of OSA-TIMS over SA-TIMS were illustrated for the analysis of structural peptide isomers (SDGRG and GRGDS $[M + H]^+$), conformational isomers (AT-hook peptide 3 KRGRGRPRK $[M + 2H]^{+2}$), and a complex mixture of polycyclic aromatic hydrocarbons (PAH) from coal tar. Baseline separation of the structural peptide isomers SDGRG and GRGDS, $[M + H]^+$, was observed, and three conformations were identified for the AT-hook peptide 3 KRGRGRPRK $[M + 2H]^{+2}$ during OSA-TIMS-FT-ICR MS. A 2-fold increase in the number of molecular features and a 2–6-fold signal-to-noise increase was observed for OSA-TIMS when compared with SA-TIMS during the PAH analysis. This work provides the proof-of-principle for further application of OSA-TIMS-FT-ICR MS for the unsupervised analysis of complex mixtures based on the characterization of the conformational space and the assignment of chemical formulas in a single analysis.



Typical operation of ultrahigh resolution mass spectrometers involves the storage of ions prior to analysis. In order to achieve very high sensitivity and resolution during FT-ICR MS measurements, the time-dependent ion signal can be measured for a very long time (tens to hundreds of seconds), thus, allowing for precise determination of the ion cyclotron frequencies.^{1,2} With the advent of new generation ICR cell designs,^{3–19} higher field magnets,^{20,21} and processing modes (e.g., absorption mode),^{22–27} the characterization of complex mixtures in a single analysis using FT-ICR MS is increasingly becoming the method of choice over shorter analysis time. The loss of coherence (dephasing) of the ion package during FT-ICR MS leads to dampening or decrease of the signal of interest, thus, limiting the sensitivity and resolution.^{28–31} This loss is typically associated with ion collisions with background molecules, inhomogeneities in the magnetic and electric field, and coalescence of the ion signal due to Coulombic interactions between the ions.^{32–35} The Coulombic interaction can also reduce the number of ions that can be effectively trapped and measured (space charge effects), thus, limiting the dynamic range and sensitivity in the analysis of complex mixtures. Previous work has shown alternatives to reduce the space charge effects in the ICR cell by changing the duration of the ionization event,³⁶ preselection of the ions of interest using a

mass analyzer,^{37,38} ejection of high abundance species,^{38–40} or selectively accumulating ions directly in the FT-ICR cell.⁴¹ Ion selection has also been performed within the FT-ICR cell utilizing phase selective excitation–de-excitation pulses, termed 2D-FT-ICR MS, in order to select and fragment target molecules by infrared multiphoton dissociation (IRMPD) or electron capture dissociation (ECD)^{42–47} or blackbody infrared radiation dissociation (BIRD).^{48–51} Alternatively, the use of gas and liquid chromatography, as well as the choice of the ionization source, has also shown an increase in sensitivity and dynamic range while typically increasing the total analyst time to tens of minutes.^{52–55}

In a different approach to effectively reduce the space charge effects, scanning and time-dispersive ion mobility spectrometry methods have been successfully coupled to FT-ICR MS.^{56–63} In particular, a low pressure drift tube based IMS (DT-IMS) was coupled to FT-ICR MS to study ion–molecule reaction chemistry.⁶² High-field asymmetric waveform ion mobility spectrometry (FA-IMS) has also been used with FT-ICR MS

Received: May 18, 2016

Accepted: June 24, 2016

Published: June 24, 2016

resulting in increased sensitivity, lower detection limits, and increased dynamic range for the analysis of poly(ethylene glycol),⁶⁰ proteins,^{57–59} and glycans⁵⁶ as a consequence of a reduction of the adverse Coulombic effects by mobility-selective injection in the FT-ICR MS. Atmospheric pressure drift tube based IMS (DT-IMS) was also successfully coupled to FT-ICR MS using a dual gate system for the separation of isomeric phosphopeptides and measurements of reduced mobility constants.⁶¹ In a recent report, we described the use of selective accumulation trapped ion mobility spectrometry (SA-TIMS) coupled to FT-ICR MS for targeted analysis of compounds of interest in complex mixtures using accurate reduced mobility ($R_{\text{IMS}} = 70\text{--}120$) and mass measurements (<10 ppb) for the case of endocrine disruptors in a complex environmental matrix.⁶³ The SA-TIMS operation is based on the trapping of a mobility range prior to injection into the FT-ICR MS; scanning of the mobility range allows for the generation of the 2D-IMS-MS plots of complex mixtures and the performance of mobility separated FT-ICR MS/MS experiments.^{63,64} While SA-TIMS-FT-ICR MS presented multiple advantages over previously reported IMS approaches, its analytical application for unsupervised molecular feature identification was mostly limited to the search for molecular formulas in the MS domain with limited identification in the IMS domain due to the number of points per mobility band (e.g., typically few points across a peak in an IMS band using a high mobility resolution scan mode).^{63,65}

In the present work, we describe for the first time the use of oversampling SA-TIMS (OSA-TIMS) coupled to FT-ICR MS. The OSA-TIMS fundamental mode of operation and their analytical application for the detection of molecular features in the IMS and MS domain are shown, as well as their advantages over previously described IMS FT-ICR MS methods. We also describe the advantages for the study of structural and conformational biomolecular isomers and the analysis of a complex mixture using unsupervised molecular feature detection. In particular, the advantages on mobility resolving power, signal-to-noise and number of molecular features determine from a 2D-IMS-MS plot are illustrated with experimental data.

EXPERIMENTAL SECTION

Materials and Reagents. A Tuning Mix calibration standard (G24221A) was obtained from Agilent Technologies (Santa Clara, CA) and used as received. The SDGRG and GRGDS and KRGRGRPRK (AT-Hook peptide 3, ATHP3) peptides were purchased from Sigma-Aldrich (St. Louis, MO) and Advanced ChemTech Inc. (Louisville, KY), respectively. All peptide standards were received as a lyophilized powder and reconstituted in 10 mM ammonium acetate in water to a final concentration of 10 μM . A standard reference material of polycyclic aromatic hydrocarbons (PAHs) in coal tar (SRM 1597a) was purchased from the National Institute of Standards and Technology (Baltimore, MA) and was diluted 1:100 in 50:50 v/v methanol/toluene. All solvents and ammonium salts utilized in this study were analytical grade or better and purchased from Fisher Scientific (Pittsburgh, PA).

Instrumentation. For this study, an orthogonal custom-built nano electrospray ionization (nanoESI) source based on a pulled glass capillary was placed on the front of a single bore, resistively coated glass capillary allowing aerodynamic focusing and desolvation of ions prior injection into the TIMS analyzer. The coal tar analysis was performed with an atmospheric

pressure photo ionization source (APPI) based on the Apollo II design (Bruker Daltonics Inc., MA) using a Kr lamp with main emission bands at 10.0 and 10.6 eV. The TIMS-FT-ICR MS instrumentation has been previously described (see details for the TIMS in Figure 1a).⁶³ Briefly, the instrument is a custom-

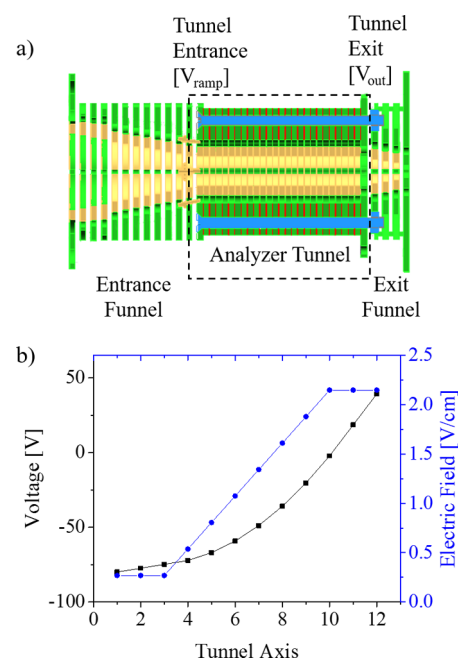


Figure 1. (a) Schematics of the TIMS cell and (b) profile of the voltage (black) and electric field (blue) across a simplified representation of the electrodes in the TIMS analyzer.

built TIMS-FT-ICR MS prototype which incorporates a TIMS analyzer that substitutes the dual funnel entrance section of a 7T Solarix FT-ICR MS spectrometer equipped with an infinity ICR cell (Bruker Daltonics Inc., MA). The TIMS cartridge is comprised of three main regions: the entrance funnel, the mobility analyzer section (tunnel), and the exit funnel, with the same RF (840 kHz and 240–280 Vpp) applied to all electrodes.^{66–68} Each electrode is divided into four electrically insulated segments, which are used to create a dipole field in the entrance and exit section to focus the ions downstream, and a quadrupolar field in the separation region to radially confine the ions during the mobility selected ion trapping. The electrodes are electrically connected through a resistive divider in order to define the electric field across the TIMS analyzer axis.

SA-TIMS versus OSA-TIMS Operation. The concept behind TIMS is the use of an electric field to hold ions stationary against a moving gas, so that the drag force is compensated by the electric field and ion packages are separated across the TIMS analyzer axis based on their mobility. Mobility selection is defined by the electric field range applied in the analyzer region; the V_{out} is typically held constant ($V_{\text{out}} = 35 \text{ V}$), while the V_{ramp} defines the mobility range that is trapped into the TIMS analyzer in each step (see Figure 1b). The mobility range that is injected into the FT-ICR MS analyzer is defined by the value of the voltage increment ΔV_{ramp} applied during a mobility step (Figure 2). The subsequent mobility range is defined by the step increment (V_{step}) in the voltage across the ramp as $\Delta V'_{\text{ramp}} = \Delta V_{\text{ramp}} + V_{\text{step}}$. During SA-TIMS operation the voltage range and the step

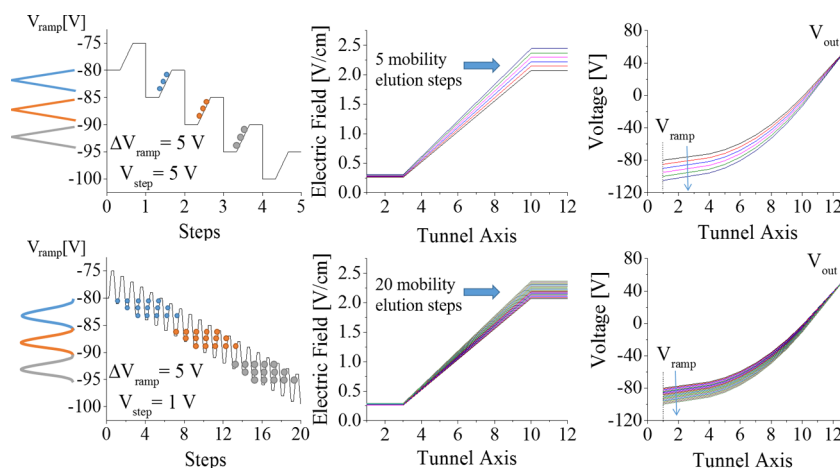


Figure 2. Comparison of the analysis sequence, electric field, and voltage applied in the TIMS analyzer during SA-TIMS (top) and OSA-TIMS (bottom) for the analysis of the same mobility range using 5 elution steps and 20 elution steps. Notice that in SA-TIMS $\Delta V_{\text{ramp}} = V_{\text{step}}$ and in OSA-TIMS $\Delta V_{\text{ramp}} > V_{\text{step}}$.

increment are the same $\Delta V_{\text{ramp}} = V_{\text{step}}$. That is, the voltage range that is scanned by V_{ramp} defines the mobility range, while the size of ΔV_{ramp} and V_{step} determines how that range is sampled. Notice that in SA-TIMS the mobility resolution is limited to the voltage range in the ramp (and in the step). A typical ΔV_{ramp} of 0.5–2 V is utilized in SA-TIMS;⁶³ the lower the range the higher the mobility resolution and the lower the sensitivity. In an alternative approach, if the $V_{\text{step}} \ll \Delta V_{\text{ramp}}$, each mobility ion package can be sampled multiple times; this mode of operation is called oversampling SA-TIMS (OSA-TIMS). During OSA-TIMS, the number of measured points can be significantly increased across a mobility ion package which enables the use of more accurate molecular feature processing tools. In addition, the mobility resolution is no longer limited to the size of the ΔV_{ramp} , is time-independent, and is mainly defined by the trapping conditions on the TIMS analyzer (e.g., bath gas velocity, electric field strength, and RF confinement).

Mobility and Collision Cross Section Calculations. The mobility of an ion can be calculated using first-principles in a TIMS analyzer.^{66–70} Each ion eluting after trapping from the TIMS cell can be described by a trapping window $E \pm \Delta E$ value that is directly related to the ion mobility $K \pm \Delta K$ and the velocity of the gas v_g . Therefore, the mobility of an ion can be described by

$$K = \frac{v_g}{E} = \frac{A}{V_{\text{elution}} - V_{\text{out}}} \quad (1)$$

where A is a calibration constant, V_{elution} is the voltage in the V_{ramp} sweep when ions elute, and V_{out} is the voltage applied to the tunnel exit. The calibration constant A was determined from previously reported mobility values for Tuning Mix calibration standard (G24221A, Agilent Technologies, Santa Clara, CA) in nitrogen (m/z 322, $K_0 = 1.376 \text{ cm}^2 \text{ V}^{-1} \text{ s}^{-1}$ and m/z 622, $K_0 = 1.013 \text{ cm}^2 \text{ V}^{-1} \text{ s}^{-1}$).⁶⁸

Reduced mobility values (K_0) were correlated with CCS (Ω) using the Mason-Schamp equation:

$$\Omega = \frac{(18\pi)^{1/2}}{16} \frac{ze}{(k_B T)^{1/2}} \left[\frac{1}{m_1} + \frac{1}{m_b} \right]^{1/2} \frac{1}{K_0 N} \quad (2)$$

where z is the charge of the ion, k_B is the Boltzmann constant, N is the number density, and m_1 and m_b refer to the masses of the ion and bath gas, respectively.⁷¹

The mobility resolving power (R) values reported herein were determined from Gaussian peak fits of the features in the TIMS distributions using OriginPro (version 8.0) by

$$R = \text{CCS}/\Delta\text{CCS} \quad (3)$$

where CCS and ΔCCS are the IMS peak center and fwhm, respectively.

Experimental Parameters. A custom-built, pulled capillary orthogonal nano electrospray ionization (nanoESI) source was utilized for the biomolecular experiments. Quartz glass capillaries (O.D.: 1.0 mm and I.D.: 0.70 mm) were pulled utilizing a P-2000 micropipette laser puller (Sutter Instruments, Novato, CA) and loaded with a 10 μL aliquot of the sample solution. A typical nanoESI source voltage of 600–1200 V was applied between the pulled capillary tips and the TIMS-FT-ICR MS instrument inlet.

An orthogonal, commercial atmospheric pressure photo-ionization (APPI) source based on the Apollo II design (Bruker Daltonics, Inc., MA) was used. Briefly, sample solutions were introduced into the nebulizer at a rate of 300 $\mu\text{L}/\text{min}$ using an external syringe pump. Typical APPI operating conditions were 900 V capillary voltage, -900 V end-cap capillary offset voltage, 2 L/min dry gas flow rate, 0.5 bar nebulizer gas pressure, a 220 $^\circ\text{C}$ dry gas temperature, and a 300 $^\circ\text{C}$ vaporizer temperature. Ions from the nanoESI and APPI source are introduced via a 0.6 mm inner diameter, single-bore glass capillary tube, which is resistively coated across its length, allowing the nebulizer to be maintained at ground potential, while the exit end of the capillary can be independently biased (typical values are 60–180 V).

TIMS separation utilized nitrogen as a bath gas at about 300 K with the gas flow velocity controlled by the pressure difference between the entrance funnel $P_1 = 2.6$ – 3.0 mbar and the exit funnel $P_2 = 1.5$ – 1.6 mbar. TIMS voltage sequences were controlled using in-house software written in National Instruments Lab VIEW (2012, V. 12.0f3) and synchronized with the FT-ICR MS acquisition program. The TIMS cell was operated using a fill/trap/elute/quench sequence of 300/50/40/10 ms, collecting a single FT-ICR MS spectrum for each mobility trapping step. FT-ICR MS operation was optimized

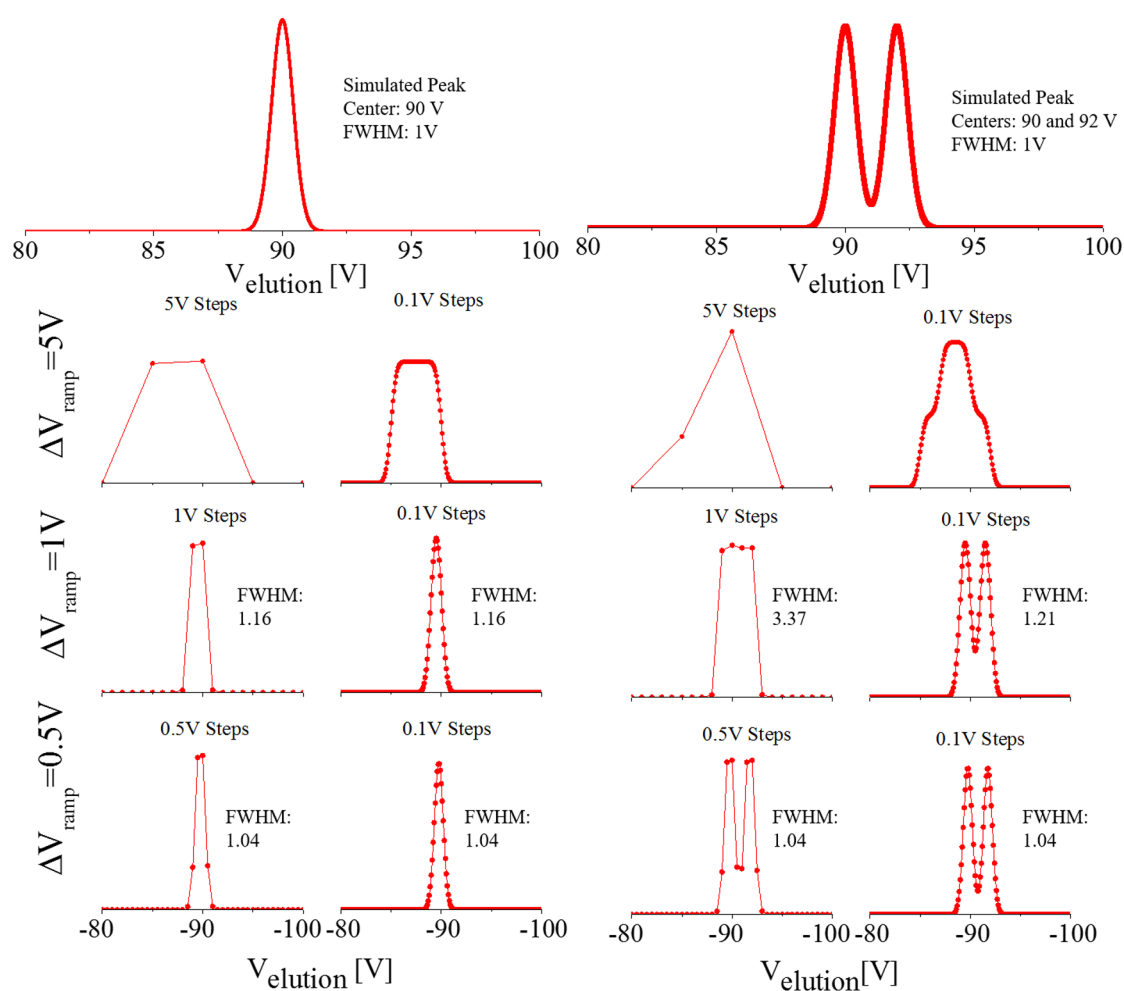


Figure 3. Theoretical IMS profiles utilizing a single and a double simulated peak with a fwhm of 1 V using selective accumulation SA (left) and oversampling OSA (right). Notice the number of points across the IMS peaks based on the trapping voltage (V_{ramp}) and the voltage steps (V_{step}): SA-TIMS $V_{ramp} = V_{step}$ and OSA-TIMS $V_{ramp} \gg V_{step}$.

for ion transmission in the m/z 300–1500 range and processed using sin-squared windowing in magnitude mode. For the evaluation of the SA-TIMS versus OSA-TIMS performance, a ΔV_{ramp} of 0.5, 1, and 5 V was used in the -25 to -180 V range, a V_{step} of 0.1, 0.2, 1, and 5 V, and single mobility experiments were accumulated in the collision cell prior to injection in the FT-ICR MS cell. The total analyst time for the SA-TIMS experiments was 73, 35, and 12 s for a ΔV_{ramp} of 0.5, 1, and 5 V compared to 5.2 min for a 400 step with 0.1 V acquisition OSA-TIMS experiments. For the analysis of the coal tar sample, multiple mobility steps (~ 30) were accumulated in the collision cell prior injection in the FT-ICR MS cell and acquired at 8–16Mword (6–12 s transient and $R_{MS} = 600$ –1200 k at $m/z = 400$, using an average of 100 scans) and 512kword ($R_{MS} = 35$ k at $m/z = 400$, using single scan) for FT-ICR MS and TIMS-FT-ICR MS analysis, respectively.

OSA-TIMS-FT-ICR MS Data Processing. For targeted analysis, the reduced number of peaks of interest permits the manual extraction of the ion mobility spectra for accurate m/z measurements (< 1 ppm) and further calibration of the OSA-TIMS scan step into mobility based on eq 1 using known mobility standards (see more details in refs 66–68). For untargeted analysis, the mobility calibration procedure is similar but the list of molecular ions of interest is generated from a

single mass spectrum acquisition during a parallel acquisition using ultrahigh resolution FT-ICR MS with multiple averaging and longer transient times (e.g., ~ 100 scan averages at 8–16Mword). The FT-ICR MS spectra are externally and internally calibrated using a Tuning Mix standard (Tunemix, G2421A, Agilent Technologies, Santa Clara, CA) and known polyaromatic hydrocarbon series, respectively. The peak lists are generated, allowing for a S/N ratio of 6. The formula calculations from the exact mass domain are performed using Data Analysis Smart Formula package (Version v. 4.2, Bruker Daltonics, CA) with a maximum formula of $C_{1-100}H_{1-100}N_{0-2}O_{0-2}S_{0-2}$, odd and even electron configurations allowed, and a mass tolerance of less than 1 ppm. The peak list is used for extraction of the ion mobility spectra from the OSA-TIMS-FT-ICR MS data set using batch processing in the data analysis package (Version v. 4.2, Bruker Daltonics, CA), followed by mobility calibration. Peak features are detected using a custom-built software package in Python v2.7 and Octave v4.0 from the mobility spectra using “asymmetric least squares smoothing” baseline correction,⁷² peak detection (“findpeak,” and “peakfit.m” functions^{73,74} using Gaussian fit functions with a fwhm criteria determined from mobility of known standards with less than 5% error as criteria

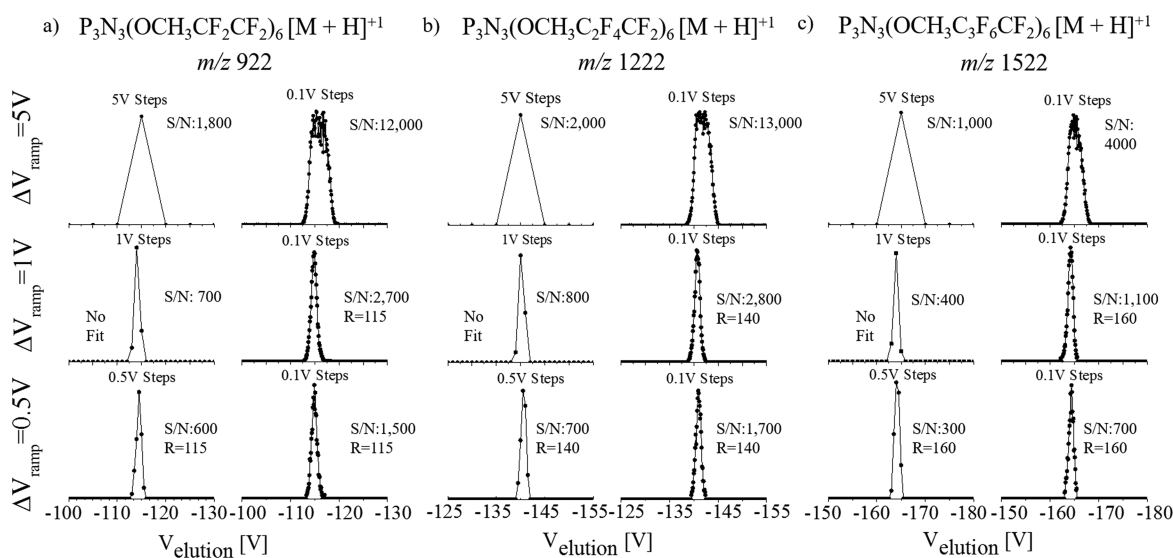


Figure 4. Typical experimental IMS profiles using selective accumulation SA (left) and oversampling OSA (right) TIMS-FT-ICR MS for the TuningMix standards at m/z (a) 922, (b) 1222, and (c) 1522. Notice the differences in resolving power and signal-to-noise ratio between SA-TIMS and OSA-TIMS.

for fit goodness), and a final generation of [m/z ; chemical formula; K; CCS] data sets.

RESULTS AND DISCUSSION

The basis for OSA-TIMS relies on the fact that during TIMS analysis ion packages are spatially resolved based on their mobilities in the TIMS analyzer axis. Then, the question arises on how one can effectively sample an ion package in the TIMS analyzer axis using discrete elution steps.^{66–68,75} Since the mobility separation in the TIMS cell is time-independent, multiple strategies can be utilized during ion trapping and elution depending on the analytical challenge. An analogy can be made between OSA-TIMS and mass spectrometry imaging (MSI). For example, in MSI ion packages are injected into the MS analyzer from spatially resolved origins during independent events and it has been previously shown that oversampling (acquiring signal from adjacent positions spaced by distances smaller than the sample probe) is routinely used to avoid undersampling and to enhance the spatial imaging resolution.^{76,77} To further illustrate the OSA-TIMS process, simulations of the OSA-TIMS read-out from a theoretical peak centered at 90 and 1 V fwhm was studied as a function of the ramp and the step size voltages (Figure 3, left). Closer inspection of Figure 3 shows that ΔV_{ramp} influences the width of the read-out peak and the step size determines the number of points across the read-out peak. When $\Delta V_{\text{ramp}} = V_{\text{step}}$ (SA-TIMS), the number of points across the read-out peak can be limited to few points if the width of the peak is on the order of the sampling step. For example, if $\Delta V_{\text{ramp}} = 5, 1,$ and 0.5 V the read-out peak has 1–2, 2–4, and 6–8 points for a 1 V fwhm simulated peak during SA-TIMS, respectively; as the ΔV_{ramp} decreases the width of the read-out peak tends to more accurately reflect the original distribution. When $V_{\text{step}} \ll \Delta V_{\text{ramp}}$ (OSA-TIMS), the number of points across the peak increases, which permits better sampling of the original peak distribution. Theoretical simulations for the case of two peaks centered around 90 and 92 V (1 V fwhm) further illustrate the OSA-TIMS read out (Figure 3, right). This case, which is equivalent to two structural/conformational isomers, shows that the two signals can only be resolved when $\Delta V_{\text{ramp}} = 0.5$ V

during SA-TIMS analysis or with $\Delta V_{\text{ramp}} = 1$ –3 V with OSA-TIMS, while their separation further increases as ΔV_{ramp} decreases ($\Delta V_{\text{ramp}} = 0.5$ V).

The OSA-TIMS concept was studied experimentally for the case of single and multiple mobility bands using known standards (Tuning Mix calibration standard m/z 922, m/z 1222, and m/z 1522), structural peptide isomers (SDGRG and GRGDS reverse peptides) and conformational peptide isomers (ATHP-3). Good agreement was observed between the theoretical and the experimental single mobility bands (see Figures 3, left, and 4). Closer inspection of the Tuning Mix mobility spectra shows similar trends for the three m/z considered as a function of the ΔV_{ramp} and ΔV_{step} during SA-TIMS and OSA-TIMS (Figure 4). For example, the analyses showed a single band for all conditions considered; that is, no artifacts are introduced during OSA-TIMS. As the ΔV_{ramp} decreases a better agreement is observed between the peak shapes from SA-TIMS and OSA-TIMS mode of operations, without compromising the resolving power. However, the ΔV_{ramp} decrease is accompanied by a ~ 3 -fold decrease in the signal-to-noise ratio from $\Delta V_{\text{ramp}} = 5$ to 0.5 V, while the signal-to-noise in the OSA-TIMS is typically 3–6 \times larger than in SA-TIMS. Notice that the number of points across the mobility band becomes analytically significant during OSA-TIMS (e.g., 15–21 points across a peak) with a $\Delta V_{\text{ramp}} = 1$ –2 V, while it may be challenging during SA-TIMS analysis (e.g., $\Delta V_{\text{ramp}} = \Delta V_{\text{step}}$).

The comparison of the theoretical and experimental profiles for multiple band mobilities also shows a good agreement (see Figures 3, right, and 5). The analysis of structural peptide isomers SDGRG and GRGDS, $[M + H]^+$, showed that they can be baseline resolved using SA-TIMS and OSA-TIMS by increasing the velocity of the gas and optimization of the RF amplitude. During OSA-TIMS for the lower $\Delta V_{\text{ramp}} = 0.5$ –1 V, no artifacts were observed and a mobility resolving power of up to 250 (CCS/ Δ CCS) was detected. Moreover, notice that there are no changes for the trapping values as a function of the ΔV_{ramp} ($<1\%$), which permits accurate ion-neutral collision cross section calculations using first-principles (see eqs 1 and 2); collision cross sections of 200 and 203 \AA^2 were detected for

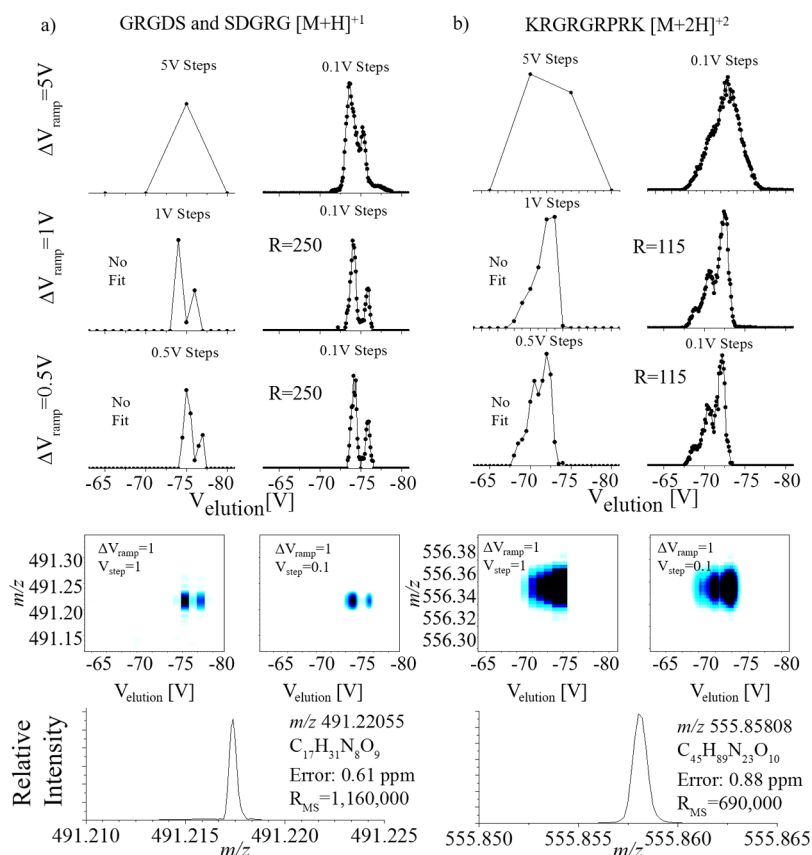


Figure 5. Typical IMS profiles using SA-TIMS (left) and OSA-TIMS (right) FT-ICR MS for (a) structural (SDGRG and GRGDS) and (b) conformational (ATHP 3) peptide isomers. Notice the high mass accuracy of the FT-ICR MS measurements.

GRGDS and SDGRG $[M + H]^+$ ions, in good agreement with previously reported values utilizing other IMS variants.^{78,79} The analysis of ATHP-3, $[M + 2H]^{+2}$, shows the potential of OSA-TIMS for the separation of conformational isomers without introducing artifacts (see Figure 5b). The detection and recognition of conformational peptide isomers during IMS analysis is challenging because there are dependencies on the solution starting conditions, molecular ion generation, and desolvation process, introduction into the IMS cell, IMS bath gas composition, and effective ion temperature during IMS separation.^{80–92} That is, in the case of conformational isomers the observation of multiple mobility bands has the prerequisite that (i) the conformational isomers were generated prior to IMS analysis and that they are stable during the IMS analysis (i.e., ions are thermalized to local minima in the free energy landscape during the IMS analysis) or (ii) conformational interconversion are energetically allowed during the IMS experiment. In any case, the mobility resolution plays a major role in the possibility to discern conformational isomers. For example, the structural flexibility of the biomolecule and the potential of conformational interconversion determines the mobility bandwidth; that is, the mobility bandwidth changes from case to case and a universal mobility bandwidth cannot be defined unless conformational interconversions are restricted during the IMS analysis. The major challenge during the study of conformational isomers is typically the assignment of mobility bands. Inspection of the ATHP-3, $[M + 2H]^{+2}$, during SA-TIMS analysis showed that the conformational space can be characterized by a broad mobility band distribution. Moreover, when the same molecular ion population was

characterized using OSA-TIMS, the increase in the mobility resolution and number of points across the peak, by decreasing the $\Delta V_{\text{ramp}} = 0.5–1$ V with a small $\Delta V_{\text{step}} = 0.1$ V, allowed the detection of three mobility bands with a resolving power of up to 120. Notice that, in the process of reducing the ΔV_{ramp} values, changes in the trapping conditions did not occur, thus, allowing accurate CCS measurements without inducing changes in the distribution of the conformational isomers.

In addition to the previously described advantages of OSA-TIMS over traditional SA-TIMS when coupled to FT-ICR MS, one of the major analytical advantages of OSA-TIMS-FT-ICR MS architecture is the possibility to identify molecular features based on the mobility and m/z domain. The ultrahigh mass resolution of the FT-ICR MS analyzers allows for the unsupervised generation of chemical formulas from complex mixtures based on the high m/z separation and mass accuracy (<1 ppm). When this is complemented with IMS separation and accurate CCS measurements, the OSA-TIMS-FT-ICR MS architecture allows for the unsupervised generation of candidate structures (see example in reference⁶⁵). This requires the separation of structural/conformational isomers using IMS, measuring the CCS, and assigning a chemical formula based on the MS measurement. The performance of OSA-TIMS-FT-ICR MS versus SA-TIMS-FT-ICR MS was evaluated for the analysis of a complex mixture of PAHs from coal tar (see Figure 6 and Table 1).

Dissection of the 2D-IMS-MS plots shows the increase in the number of molecular features detected from 2000 to 2800 and to 3800, comparing FT-ICR MS to SA-TIMS-FT-ICR MS and to OSA-TIMS-FT-ICR MS, respectively (see Figure S1).

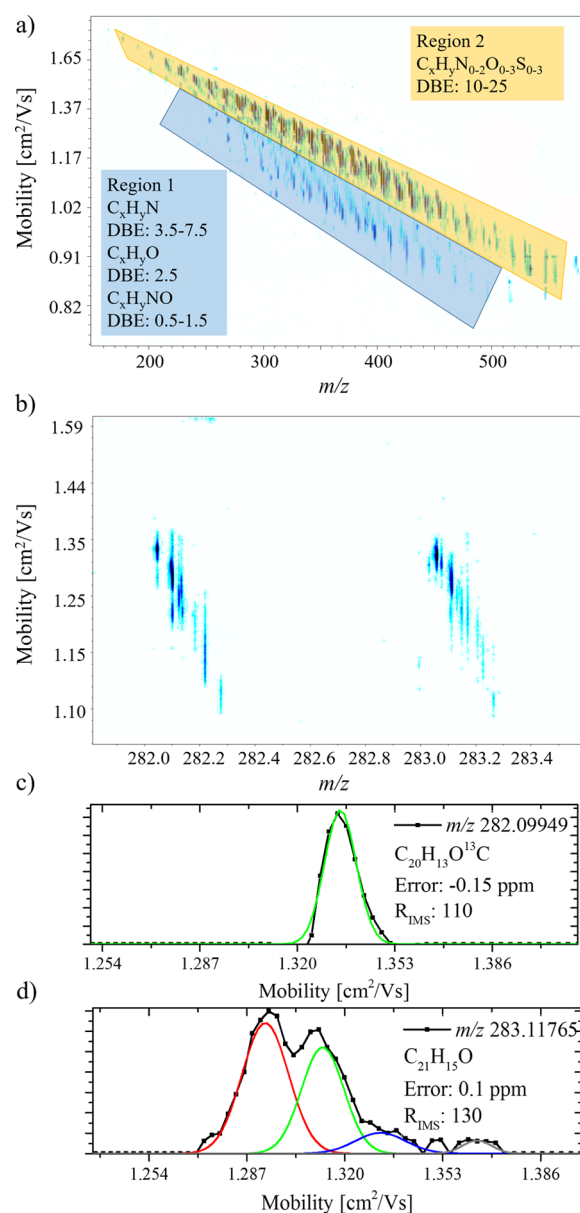


Figure 6. (a) Typical 2D-IMS-MS contour plot obtained using APPI-OSA-TIMS-FT-ICR MS from a complex mixture of coal tar. Two regions of interest are clearly discernible, resulting in a more aliphatic region (blue) and a more aromatic region (gold). (b) A closer view of m/z 282–284 is shown, as well as the unsupervised fits for (c) a single and (d) multiple mobility band distributions.

Inspection of the 2D-IMS-MS of coal tar shows two main trend lines (regions 1 and 2 in Figure 6a). The separation of regions 1 and 2 in the IMS-MS space reduces the chemical noise and permits the generation of region specific MS projections of signals with lower abundance (e.g., see Figure S2 where region 2 compounds are an order of magnitude less abundant than those detected in region 1). That is, this reduction in space charge effects and the increased peak capacity allows for greater sensitivity for the lower abundance species. Region 1 is composed primarily of a nitrogen containing compounds with a DBE 3.5–7.5, corresponding to alkyl pyridines and larger aromatics (e.g., phenyl-pyridine), as well as less-saturated molecules. Region 2 is composed primarily of aromatic and more condensed structures with a DBE range of 10–25. While SA-TIMS-FT-ICR MS represents an advantage over alternative

Table 1. List of Compounds Assigned Based on the Accurate Mass and Mobility from the 2D-IMS-MS Contour Plot Obtained Using APPI-OSA-TIMS-FT-ICR MS from a Complex Mixture of Coal Tar

m/z	ion formula	error (ppm)	mobility [$\text{cm}^2/(\text{V s})$]
282.04981	$\text{C}_{20}\text{H}_{10}\text{S}$	−0.1	1.365
282.09949	$\text{C}_{20}\text{H}_{13}\text{O}^{13}\text{C}$	−0.1	1.335
282.10394	$\text{C}_{21}\text{H}_{14}\text{O}$	−0.09	1.121
			1.250
			1.301
			1.314
282.12775	$\text{C}_{21}\text{H}_{16}\text{N}$	−0.1	1.142
			1.269
			1.286
282.13587	$\text{C}_{21}\text{H}_{17}^{13}\text{C}$	−0.1	1.224
			1.285
			1.306
282.14035	$\text{C}_{22}\text{H}_{18}$	−0.18	1.253
282.22166	$\text{C}_{20}\text{H}_{28}\text{N}$	−0.1	1.090
			1.160
			1.183
			1.206
282.27914	$\text{C}_{18}\text{H}_{36}\text{NO}$	−0.01	1.120
			1.132
			1.228
283.05763	$\text{C}_{20}\text{H}_{11}\text{S}$	−0.1	1.352
283.07541	$\text{C}_{20}\text{H}_{11}\text{O}_2$	−0.2	1.339
283.10508	$\text{C}_{20}\text{H}_{14}\text{O}^{13}\text{C}$	0.9	1.250
283.11176	$\text{C}_{21}\text{H}_{15}\text{O}$	−0.1	1.293
			1.314
			1.332
			1.364
283.13105	$\text{C}_{20}\text{H}_{16}\text{N}^{13}\text{C}$	0.1	1.269
283.14817	$\text{C}_{22}\text{H}_{19}$	−0.2	1.151
			1.245
			1.264
283.16928	$\text{C}_{18}\text{H}_{21}\text{N}_2\text{O}$	−0.7	1.164
			1.238
			1.259
			1.339
283.26317	$\text{C}_{18}\text{H}_{35}\text{O}_2$	−0.03	1.123

strategies (e.g., parallel analysis by GCxGC-TOF, FT-ICR MS, and IMS-TOF-MS) for the separation of high mass isobars and isomers, the major drawback was in the possibility to separate closely related mobility bands due to the reduced number of points across the peak. With the introduction of OSA-TIMS-FT-ICR MS, the higher confidence of peak assignment during unsupervised processing of 2D-IMS-MS data permits the generation of (m/z ; chemical formula; K; CCS) data sets from a single analysis. Unsupervised processing of the OSA-TIMS analysis of the coal tar mixture allows the detection of 3800 molecular features from 1800 assigned formulas. This is illustrated for the case of two mobility distributions between m/z 282–284 (see Figure 6b–d). In this case, the increased number of points allows the automated peak fitting tools to accurately determine the profile for single and for multiple mobility band distributions (see example in Figure 6c,d).

Notice that the specifics of OSA-TIMS-FT-ICR MS analysis (and corresponding analysis time) can be tailored by the sample complexity and relative abundance of the molecular features of interest. That is, the time-independent nature of the

OSA-TIMS separation allows for the selective analysis of the mobility space of interest with varying degrees of mobility resolution and number of points across the peak; the higher the resolution and number of peaks, the longer the analysis time. In the case of the analysis of the coal tar by OSA-TIMS-FT-ICR MS, the analysis was completed in 85 min. In addition, as shown in the case of the PAH analysis, the number of OSA-TIMS steps that are accumulated and injected into the ICR cell can be tailored, which allows for better optimization of the ICR parameters, leading to higher mass resolution and better mass accuracy.

CONCLUSIONS

During TIMS analysis, ion packages are spatially resolved based on their mobilities along the TIMS analyzer axis and multiple strategies can be utilized to optimized the analytical applicability. In the present paper, we described the fundamentals and applicability of OSA-TIMS when coupled to ultrahigh resolution mass analyzers (e.g., FT-ICR MS). In particular, the analytical advantages during the analysis of structural/conformational isomers as well as for the unsupervised analysis of complex mixtures utilizing the mobility and m/z domain were illustrated. Results showed that accurate ion-neutral collision cross sections (<1%) can be measured using OSA-TIMS-FT-ICR MS with high mobility resolving powers (R_{IMS} up to 250), high mass accuracy (<1 ppm), and ultrahigh mass resolution (R_{MS} up to 600–1200k at m/z 400) in a single analysis. A 2-fold increase in the number of molecular features and a 2–6-fold signal-to-noise increase were observed for OSA-TIMS when compared with SA-TIMS. This work provides the proof-of-principle for further application of OSA-TIMS-FT-ICR MS for the unsupervised analysis of complex mixtures based on the characterization of the conformational space and the assignment of chemical formulas in a single analysis.

ASSOCIATED CONTENT

Supporting Information

The Supporting Information is available free of charge on the ACS Publications website at DOI: 10.1021/acs.analchem.6b01946.

Additional information as noted in the text (Figures S-1 and S-2; PDF).

AUTHOR INFORMATION

Corresponding Author

*Ph.: 305-348-2037. Fax: 305-348-3772. E-mail: fernandf@fiu.edu.

Notes

The authors declare no competing financial interest.

ACKNOWLEDGMENTS

This work was supported by National Institute of Health (Grant No. R00GM106414 to F.F.-L.). The authors would like to acknowledge the helpful discussion with Dr. Tom C. O'Haver (UMD) and Mr. Steven Silvester (Oct2PY) during the development of the 2D-IMS-MS processing tools. The authors will also like to acknowledge the helpful discussions and technical support from Dr. Mark E. Ridgeway, Dr. Christopher J. Thompson, and Dr. Melvin A. Park from Bruker Daltonics Inc. during the development and installation of the custom-built TIMS-FT-ICR MS instrument.

REFERENCES

- (1) Xian, F.; Hendrickson, C. L.; Marshall, A. G. *Anal. Chem.* **2012**, *84*, 708–719.
- (2) Nikolaev, E. N.; Kostyukevich, Y. I.; Vladimirov, G. N. *Mass Spectrom. Rev.* **2016**, *35*, 219–258.
- (3) Leach, F. E., III; Norheim, R.; Anderson, G.; Pasa-Tolic, L. *J. Am. Soc. Mass Spectrom.* **2014**, *25*, 2069–2072.
- (4) Boldin, I. A.; Nikolaev, E. N. *Rapid Commun. Mass Spectrom.* **2011**, *25*, 122–126.
- (5) Frankevich, V.; Zenobi, R. *Int. J. Mass Spectrom.* **2001**, *207*, 57–67.
- (6) Weisbrod, C. R.; Kaiser, N. K.; Skulason, G. E.; Bruce, J. E. *Anal. Chem.* **2010**, *82*, 6281–6286.
- (7) Weisbrod, C. R.; Kaiser, N. K.; Skulason, G. E.; Bruce, J. E. *Anal. Chem.* **2008**, *80*, 6545–6553.
- (8) Brustkern, A. M.; Rempel, D. L.; Gross, M. L. *J. Am. Soc. Mass Spectrom.* **2008**, *19*, 1281–1285.
- (9) Brustkern, A. M.; Rempel, D. L.; Gross, M. L. *J. Am. Soc. Mass Spectrom.* **2010**, *21*, 451–454.
- (10) Nikolaev, E. N.; Boldin, I. A.; Jertz, R.; Baykut, G. *J. Am. Soc. Mass Spectrom.* **2011**, *22*, 1125–1133.
- (11) Kostyukevich, Y. I.; Vladimirov, G. N.; Nikolaev, E. N. *J. Am. Soc. Mass Spectrom.* **2012**, *23*, 2198–2207.
- (12) Kaiser, N. K.; Savory, J. J.; McKenna, A. M.; Quinn, J. P.; Hendrickson, C. L.; Marshall, A. G. *Anal. Chem.* **2011**, *83*, 6907–6910.
- (13) Tolmachev, A. V.; Robinson, E. W.; Wu, S.; Smith, R. D.; Pasa-Toli, L. *J. Am. Soc. Mass Spectrom.* **2011**, *22*, 1334–1342.
- (14) Tolmachev, A. V.; Robinson, E. W.; Wu, S.; Pasa-Tolic, L.; Smith, R. D. *Int. J. Mass Spectrom.* **2009**, *287*, 32–38.
- (15) Tolmachev, A. V.; Robinson, E. W.; Smith, R. D.; Leach, F. E.; Futrell, J. H.; Paša-Tolić, L. *Int. J. Mass Spectrom.* **2012**, *325*, 45–50.
- (16) Nagornov, K. O.; Kozhinov, A. N.; Tsybin, O. Y.; Tsybin, Y. O. *J. Am. Soc. Mass Spectrom.* **2015**, *26*, 741–751.
- (17) Tolmachev, A. V.; Robinson, E. W.; Wu, S.; Kang, H.; Lourette, N. M.; Pasa-Tolic, L.; Smith, R. D. *J. Am. Soc. Mass Spectrom.* **2008**, *19*, 586–597.
- (18) Tolmachev, A. V.; Robinson, E. W.; Wu, S.; Smith, R. D.; Futrell, J. H.; Pasa-Tolic, L. *J. Am. Soc. Mass Spectrom.* **2012**, *23*, 1169–1172.
- (19) Popov, I. A.; Nagornov, K.; Vladimirov, G. N.; Kostyukevich, Y. I.; Nikolaev, E. N. *J. Am. Soc. Mass Spectrom.* **2014**, *25*, 790–799.
- (20) Marshall, A. G.; Guan, S. *Rapid Commun. Mass Spectrom.* **1996**, *10*, 1819–1823.
- (21) Hendrickson, C. L.; Quinn, J. P.; Kaiser, N. K.; Smith, D. F.; Blakney, G. T.; Chen, T.; Marshall, A. G.; Weisbrod, C. R.; Beu, S. C. *J. Am. Soc. Mass Spectrom.* **2015**, *26*, 1626–1632.
- (22) Cho, Y.; Qi, Y.; O'Connor, P. B.; Barrow, M. P.; Kim, S. *J. Am. Soc. Mass Spectrom.* **2014**, *25*, 154–157.
- (23) Qi, Y.; Li, H.; Wills, R. H.; Perez-Hurtado, P.; Yu, X.; Kilgour, D. P.; Barrow, M. P.; Lin, C.; O'Connor, P. B. *J. Am. Soc. Mass Spectrom.* **2013**, *24*, 828–834.
- (24) Qi, Y.; Witt, M.; Jertz, R.; Baykut, G.; Barrow, M. P.; Nikolaev, E. N.; O'Connor, P. B. *Rapid Commun. Mass Spectrom.* **2012**, *26*, 2021–2026.
- (25) Qi, Y.; Barrow, M. P.; Li, H.; Meier, J. E.; Van Orden, S. L.; Thompson, C. J.; O'Connor, P. B. *Anal. Chem.* **2012**, *84*, 2923–2929.
- (26) Kilgour, D. P.; Nagornov, K. O.; Kozhinov, A. N.; Zhurov, K. O.; Tsybin, Y. O. *Rapid Commun. Mass Spectrom.* **2015**, *29*, 1087–1093.
- (27) Kilgour, D. P.; Wills, R.; Qi, Y.; O'Connor, P. B. *Anal. Chem.* **2013**, *85*, 3903–3911.
- (28) Nakata, M. T.; Hart, G. W.; Peterson, B. G. *J. Am. Soc. Mass Spectrom.* **2010**, *21*, 1712–1719.
- (29) Mitchell, D. W.; Smith, R. D. *Phys. Rev. E: Stat. Phys., Plasmas, Fluids, Relat. Interdiscip. Top.* **1995**, *52*, 4366–4386.
- (30) Boldin, I. A.; Nikolaev, E. N. *Rapid Commun. Mass Spectrom.* **2009**, *23*, 3213–3219.
- (31) Nikolaev, E. N. *Int. J. Mass Spectrom.* **2015**, *377*, 421–431.

- (32) Comisarow, M. B.; Marshall, A. G. *J. Chem. Phys.* **1976**, *64*, 110–119.
- (33) Guan, S.; Li, G.-Z.; Marshall, A. G. *Int. J. Mass Spectrom. Ion Processes* **1997**, *167*, 185–193.
- (34) Mitchell, D. W. *J. Am. Soc. Mass Spectrom.* **1999**, *10*, 136–152.
- (35) Nikolaev, E. N.; Heeren, R. M.; Popov, A. M.; Pozdnev, A. V.; Chingina, K. S. *Rapid Commun. Mass Spectrom.* **2007**, *21*, 3527–3546.
- (36) Stafford, G. C., Jr; Taylor, D. M.; Bradshaw, S. C. *US5107109 A*, 1992.
- (37) Senko, M. W.; Hendrickson, C. L.; Emmett, M. R.; Shi, S. D.-H.; Marshall, A. G. *J. Am. Soc. Mass Spectrom.* **1997**, *8*, 970–976.
- (38) Belov, M. E.; Anderson, G. A.; Angell, N. H.; Shen, Y.; Tolic, N.; Udseth, H. R.; Smith, R. D. *Anal. Chem.* **2001**, *73*, 5052–5060.
- (39) Paša-Tolić, L.; Harkewicz, R.; Anderson, G. A.; Tolić, N.; Shen, Y.; Zhao, R.; Thrall, B.; Masselon, C.; Smith, R. D. *J. Am. Soc. Mass Spectrom.* **2002**, *13*, 954–963.
- (40) Harkewicz, R.; Belov, M. E.; Anderson, G. A.; Pasa-Tolic, L.; Masselon, C. D.; Prior, D. C.; Udseth, H. R.; Smith, R. D. *J. Am. Soc. Mass Spectrom.* **2002**, *13*, 144–154.
- (41) Bruce, J. E.; Anderson, G. A.; Hofstadler, S. A.; Van Orden, S. L.; Sherman, M. S.; Rockwood, A. L.; Smith, R. D. *Rapid Commun. Mass Spectrom.* **1993**, *7*, 914–919.
- (42) van Aghoven, M. A.; Barrow, M. P.; Chiron, L.; Coutouly, M. A.; Kilgour, D.; Wootton, C. A.; Wei, J.; Soulby, A.; Delsuc, M. A.; Rolando, C.; O'Connor, P. B. *J. Am. Soc. Mass Spectrom.* **2015**, *26*, 2105–2114.
- (43) van Aghoven, M. A.; Chiron, L.; Coutouly, M. A.; Delsuc, M. A.; Rolando, C. *Anal. Chem.* **2012**, *84*, 5589–5595.
- (44) van Aghoven, M. A.; Chiron, L.; Coutouly, M.-A.; Sehgal, A. A.; Pelupessy, P.; Delsuc, M.-A.; Rolando, C. *Int. J. Mass Spectrom.* **2014**, *370*, 114–124.
- (45) van Aghoven, M. A.; Delsuc, M. A.; Bodenhausen, G.; Rolando, C. *Anal. Bioanal. Chem.* **2013**, *405*, 51–61.
- (46) van Aghoven, M. A.; Delsuc, M.-A.; Rolando, C. *Int. J. Mass Spectrom.* **2011**, *306*, 196–203.
- (47) van Aghoven, M. A.; Wootton, C. A.; Chiron, L.; Coutouly, M. A.; Soulby, A.; Wei, J.; Barrow, M. P.; Delsuc, M. A.; Rolando, C.; O'Connor, P. B. *Anal. Chem.* **2016**, *88*, 4409–4417.
- (48) Dunbar, R. C. *Mass Spectrom. Rev.* **2004**, *23*, 127–158.
- (49) Laskin, J. *Principles of Mass Spectrometry Applied to Biomolecules*; John Wiley & Sons, Inc.: Hoboken, NJ, U.S.A., 2006; pp 619–665.
- (50) Klassen, J. S.; Schnier, P. D.; Williams, E. R. *J. Am. Soc. Mass Spectrom.* **1998**, *9*, 1117–1124.
- (51) Felitsyn, N.; Kitova, E. N.; Klassen, J. S. *Anal. Chem.* **2001**, *73*, 4647–4661.
- (52) Barrow, M. P.; Peru, K. M.; Headley, J. V. *Anal. Chem.* **2014**, *86*, 8281–8288.
- (53) Lababidi, S.; Panda, S. K.; Andersson, J. T.; Schrader, W. *Anal. Chem.* **2013**, *85*, 9478–9485.
- (54) Lababidi, S.; Schrader, W. *Rapid Commun. Mass Spectrom.* **2014**, *28*, 1345–1352.
- (55) Benigni, P.; DeBord, J. D.; Thompson, C. J.; Gardinali, P.; Fernandez-Lima, F. *Energy Fuels* **2016**, *30*, 196–203.
- (56) Kailemia, M. J.; Park, M.; Kaplan, D. A.; Venot, A.; Boons, G. J.; Li, L.; Linhardt, R. J.; Amster, I. J. *J. Am. Soc. Mass Spectrom.* **2014**, *25*, 258–268.
- (57) Robinson, E. W.; Leib, R. D.; Williams, E. R. *J. Am. Soc. Mass Spectrom.* **2006**, *17*, 1469–1479.
- (58) Robinson, E. W.; Sellon, R. E.; Williams, E. R. *Int. J. Mass Spectrom.* **2007**, *259*, 87–95.
- (59) Robinson, E. W.; Williams, E. R. *J. Am. Soc. Mass Spectrom.* **2005**, *16*, 1427–1437.
- (60) Robinson, E. W.; Garcia, D. E.; Leib, R. D.; Williams, E. R. *Anal. Chem.* **2006**, *78*, 2190–2198.
- (61) Tang, X.; Bruce, J. E.; Hill, H. H., Jr. *Rapid Commun. Mass Spectrom.* **2007**, *21*, 1115–1122.
- (62) Bluhm, B. K.; Gillig, K. J.; Russell, D. H. *Rev. Sci. Instrum.* **2000**, *71*, 4078–4086.
- (63) Benigni, P.; Thompson, C. J.; Ridgeway, M. E.; Park, M. A.; Fernandez-Lima, F. *Anal. Chem.* **2015**, *87*, 4321–4325.
- (64) Pu, Y.; Ridgeway, M. E.; Glaskin, R. S.; Park, M. A.; Costello, C. E.; Lin, C. *Anal. Chem.* **2016**, *88*, 3440–3443.
- (65) Benigni, P.; Marin, R.; Fernandez-Lima, F. *Int. J. Ion Mobility Spectrom.* **2015**, *18*, 151–157.
- (66) Fernandez-Lima, F. A.; Kaplan, D. A.; Park, M. A. *Rev. Sci. Instrum.* **2011**, *82*, 126106.
- (67) Fernandez-Lima, F.; Kaplan, D. A.; Suetering, J.; Park, M. A. *Int. J. Ion Mobility Spectrom.* **2011**, *14*, 93–98.
- (68) Hernandez, D. R.; DeBord, J. D.; Ridgeway, M. E.; Kaplan, D. A.; Park, M. A.; Fernandez-Lima, F. *Analyst* **2014**, *139*, 1913–1921.
- (69) Benigni, P.; Marin, R.; Molano-Arevalo, J. C.; Garabedian, A.; Wolff, J. J.; Ridgeway, M. E.; Park, M. A.; Fernandez-Lima, F. *Int. J. Ion Mobility Spectrom.* **2016**, 1–10.
- (70) Adams, K. J.; Montero, D.; Aga, D.; Fernandez-Lima, F. *Int. J. Ion Mobility Spectrom.* **2016**, 1–8.
- (71) McDaniel, E. W.; Mason, E. A. *Mobility and Diffusion of Ions in Gases*; John Wiley and Sons, Inc., New York, 1973; p 381.
- (72) Eilers, P. H.; Boelens, H. F. *Leiden University Medical Centre Report*, 2005.
- (73) O'Haver, T. A. *Pragmatic Introduction to Signal Processing*, 2nd ed.; Self published, Printed by CreateSpace Independent Publishing Platform, 2016.
- (74) Thomas C, O. H. Interactive Peak Fitter, <https://terpconnect.umd.edu/~toh/spectrum/InteractivePeakFitter.htm> (accessed Apr, 11, 2016).
- (75) Ridgeway, M. E.; Wolff, J. J.; Silveira, J. A.; Lin, C.; Costello, C. E.; Park, M. A. *Int. J. Ion Mobility Spectrom.* **2016**, 1–9.
- (76) Todd, P. J.; Schaaff, T. G.; Chaurand, P.; Caprioli, R. M. *J. Mass Spectrom.* **2001**, *36*, 355–369.
- (77) Jurchen, J. C.; Rubakhin, S. S.; Sweedler, J. V. *J. Am. Soc. Mass Spectrom.* **2005**, *16*, 1654–1659.
- (78) Giles, K.; Williams, J. P.; Campuzano, I. *Rapid Commun. Mass Spectrom.* **2011**, *25*, 1559–1566.
- (79) Bush, M. F.; Hall, Z.; Giles, K.; Hoyes, J.; Robinson, C. V.; Ruotolo, B. T. *Anal. Chem.* **2010**, *82*, 9557–9565.
- (80) Schenk, E. R.; Almeida, R.; Miksovskaja, J.; Ridgeway, M. E.; Park, M. A.; Fernandez-Lima, F. *J. Am. Soc. Mass Spectrom.* **2015**, *26*, 555–563.
- (81) McKenzie-Coe, A.; DeBord, J. D.; Ridgeway, M.; Park, M.; Eiceman, G.; Fernandez-Lima, F. *Analyst* **2015**, *140*, 5692–5699.
- (82) Schenk, E. R.; Ridgeway, M. E.; Park, M. A.; Leng, F.; Fernandez-Lima, F. *Anal. Chem.* **2014**, *86*, 1210–1214.
- (83) Molano-Arevalo, J. C.; Hernandez, D. R.; Gonzalez, W. G.; Miksovskaja, J.; Ridgeway, M. E.; Park, M. A.; Fernandez-Lima, F. *Anal. Chem.* **2014**, *86*, 10223–10230.
- (84) Fernandez-Lima, F. A.; Wei, H.; Gao, Y. Q.; Russell, D. H. *J. Phys. Chem. A* **2009**, *113*, 8221–8234.
- (85) Morsa, D.; Gabelica, V.; De Pauw, E. *J. Am. Soc. Mass Spectrom.* **2014**, *25*, 1384–1393.
- (86) Morsa, D.; Gabelica, V.; De Pauw, E. *Anal. Chem.* **2011**, *83*, 5775–5782.
- (87) Shi, L.; Holliday, A. E.; Glover, M. S.; Ewing, M. A.; Russell, D. H.; Clemmer, D. E. *J. Am. Soc. Mass Spectrom.* **2016**, *27*, 22–30.
- (88) Shi, H.; Clemmer, D. E. *J. Phys. Chem. B* **2014**, *118*, 3498–3506.
- (89) Silveira, J. A.; Fort, K. L.; Kim, D.; Servage, K. A.; Pierson, N. A.; Clemmer, D. E.; Russell, D. H. *J. Am. Chem. Soc.* **2013**, *135*, 19147–19153.
- (90) Shi, H.; Pierson, N. A.; Valentine, S. J.; Clemmer, D. E. *J. Phys. Chem. B* **2012**, *116*, 3344–3352.
- (91) Pierson, N. A.; Chen, L.; Valentine, S. J.; Russell, D. H.; Clemmer, D. E. *J. Am. Chem. Soc.* **2011**, *133*, 13810–13813.
- (92) Pierson, N. A.; Valentine, S. J.; Clemmer, D. E. *J. Phys. Chem. B* **2010**, *114*, 7777–7783.